Front. Phys. 13(5), 134208 (2018)
https://doi.org/10.1007/s11467-018-0817-8

RESEARCH ARTICLE

Three-dimensional atom localization via spontaneous emission in a four-level atom

Fei Song, Jin-Yu Chen, Zhi-Ping Wang†, Ben-Li Yu

Key Laboratory of Opto-Electronic Information Acquisition and Manipulation of Ministry of Education, Anhui University, Hefei 230601, China
Corresponding author. E-mail: †wzping@mail.ustc.edu.cn
Received February 17, 2018; accepted June 23, 2018

We investigate high-precision three-dimensional (3D) atom localization in a coherently-driven, four-level atomic system via spontaneous emission. Space-dependent atom-field interactions allow atomic position information to be obtained by measuring spontaneous emission. By properly varying system parameters, atoms within a certain range can be localized with nearly a probability of 100% and a maximal resolution of $\sim 0.04\lambda$. This scheme may be useful for the high-precision measurement of the center-of-mass wave functions of moving atoms and in atom nanolithography.

Keywords atom localization, spontaneous emission, dressed-state picture

PACS numbers 42.50.Gy, 32.80.Qk

1 Introduction

Spontaneous emission is a well-known fundamental process that results from the interaction between radiation and matter. It has been shown that spontaneous emission can create quantum interference [1], which is usually referred to as spontaneously generated coherence (SGC). Moreover, SGC has been predicted to lead to many interesting phenomena [2–12], such as dark lines in spontaneous emission spectra, the enhancement, narrowing, suppression, or complete cancellation of spontaneous emission, and phase-sensitive spontaneous emission and absorption spectra. Recently, based on SGC, many schemes have been proposed for atom localization. For instance, Zubairy and colleagues discussed one-dimensional (1D) atom localization using resonance fluorescence and phase, with the detection of a spontaneously emitted photon possible due to its interaction with a classical standing-wave field and its reservoir modes [13–16]. Wan and co-workers suggested two-dimensional (2D) atom localization based on controlled spontaneous emission [17, 18]. Ding and colleagues proposed a scheme for 2D atom localization via spontaneous emission in a coherently driven, five-level, M-type atomic system [19] and via the controlled spontaneous emission from a driven cyclic-configuration atomic system [20]. More recently, we have reported two three-dimensional (3D) atom localization schemes using spontaneous emission [21–23].

In this article, we demonstrate 3D atom localization in a four-level atomic system via spontaneous emission. Recently, several 3D atom localization schemes have been proposed using three mutually perpendicular standing-wave fields [24–28]. However, the approach outlined here differs significantly from previous schemes. First, we show that high-precision and high-resolution 3D atom localization can be realized by modulating system parameters that are well-understood from qualitative explanations of the dressed-state picture. Second, we find that the localization precision and spatial resolution of an atom can be effectively modulated by the phase shifts and wave vectors of the standing-wave fields. By properly adjusting the system parameters, atoms can be localized in a particular position with a maximal resolution of $\sim 0.04\lambda$, which is better than previous schemes [21–28]. Third, with the scheme proposed here, no stringent conditions must be satisfied, making it easy to observe expected 3D atom localization phenomena related to atomic SGC with a magneto-optical trap (MOT).

2 Model and dynamic equations

We consider a four-level atomic tripod configuration as shown in Fig. 1. The configuration has three ground

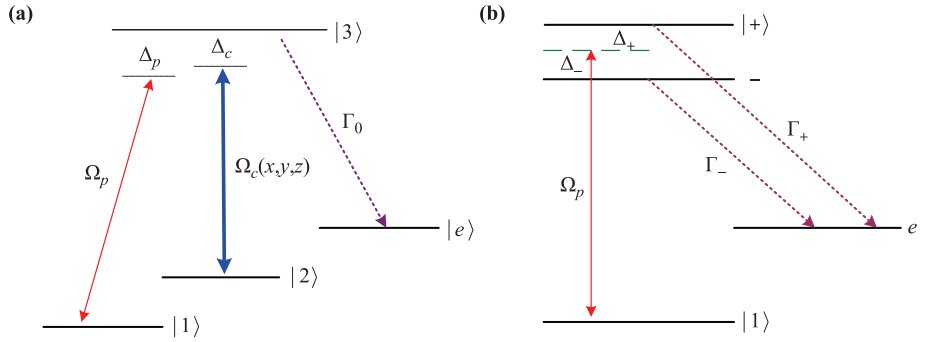

Fig. 1 **(a)** The atomic energy levels in the bare state picture. **(b)** The atomic energy levels in the dressed-state picture.

states $|1\rangle$, $|2\rangle$ and $|e\rangle$, one excited states $|3\rangle$. A weak probe field with the Rabi frequency $2\Omega_p$ is applied to the transition $|1\rangle \leftrightarrow |3\rangle$, the transition from state $|3\rangle$ to state $|e\rangle$ is assumed to be coupled by the vacuum modes in the free space, while the coupling field with position-dependent Rabi frequency Ω_c is applied to couple transition $|2\rangle \leftrightarrow |3\rangle$. In our scheme, Ω_c is the superposition of three orthogonal standing-wave fields and can be defined as [29, 30]

$$\Omega_c = \Omega_c(x) + \Omega_c(y) + \Omega_c(z), \tag{1}$$

with

$$\Omega_c(x) = \Omega_1[\sin(k_1 x + \theta_1) + \sin(k_2 x)], \tag{2a}$$
$$\Omega_c(y) = \Omega_2[\sin(k_3 y + \theta_2) + \sin(k_4 y)], \tag{2b}$$
$$\Omega_c(z) = \Omega_3[\sin(k_5 z + \theta_3) + \sin(k_6 z)], \tag{2c}$$

where $\Omega_c(x)$, $\Omega_c(y)$ and $\Omega_c(z)$ are also the superposition of two orthogonal standing-wave fields aligning along the x, y, and z directions respectively; $k_i = 2\pi/\lambda_i$ $(i = 1-6)$ is the wave vectors of the corresponding standing-wave fields, where λ_i is the wavelength of the standing-wave fields.

The interaction Hamiltonian of the atom-field system using electric-dipole and rotating-wave approximations can be defined as

$$H_I = \sum_k \{g_{k,3e}\exp(\mathrm{i}\delta_k t)b_k|3\rangle\langle e|\} + \Omega_p\exp(\mathrm{i}\Delta_p t)|3\rangle\langle 1| + \Omega_c(x,y,z)\exp(\mathrm{i}\Delta_c t)|3\rangle\langle 2| + H.c., \tag{3}$$

where g_k is the coupling constant between the $\boldsymbol{k}$th vacuum mode and the transition $|3\rangle \leftrightarrow |i\rangle$; b_k is the annihilation (creation) operator for the $\boldsymbol{k}$th vacuum mode; Δ_p, Δ_c and δ_k are the detuning of corresponding fields.

The dynamics of this system can be described by using probability amplitude equations. Then the wave function of the system at time t can be expressed in terms of the state vectors as

$$|\Psi(t)\rangle = \int \mathrm{d}x\mathrm{d}y\mathrm{d}z f(x,y,z)|x\rangle|y\rangle|z\rangle\{[A_1(x,y,z;t)|1\rangle + A_2(x,y,z;t)|2\rangle + A_3(x,y,z;t)|3\rangle]|\{0\}\rangle + \sum_k A_{e,k}(x,y,z;t)|e\rangle|1_k\rangle\}, \tag{4}$$

where $f(x,y,z)$ is the center-of-mass wave function of the atom; $A_i(x,y,z;t)$ $(i = 1,2,3)$ represents the probability amplitude to find the atom at time t; $|\{0\}\rangle$ stand for the vacuum of the radiation field.

The 3D atom localization in our scheme is based on the fact that the spontaneously emitted photon carries information about the position of atom in 3D space as a result of the spatial position-dependent atom-field interaction. When we have detected at time t a spontaneously emitted photon in the vacuum mode of wave vector $\boldsymbol{k}$, the atom is in its internal state $|e\rangle$ and the state vector of the system, after making appropriate projection over $|\Psi(t)\rangle$, is reduced to

$$|\Psi_{e,1_k}\rangle = N\langle e,1_k|\Psi(t)\rangle = \int \mathrm{d}x\mathrm{d}y\mathrm{d}z f(x,y,z)A_{e,k}(x,y,z;t)|x\rangle|y\rangle|z\rangle, \tag{5}$$

where N is a normalization constant. Thus, the conditional position probability distribution, i.e. the probability of finding the atom in 3D space at time t is

$$W(x,y,z;t|e,1_k) = |N|^2|\langle x|\langle y|\langle z|\Psi_{e,1_k}\rangle||^2 = |N|^2|f(x,y,z)|^2|A_{e,1_k}(x,y,z;t)|^2, \tag{6}$$

here $W(x,y,z;t|e,1_k)$ is the conditional position probability distribution, which follows from the probability amplitude $A_{e,1_k}(x,y,z;t)$.

By using the Weisskopf–Wigner theory, the following dynamical equations for atomic probability amplitudes

are given by

$$\mathrm{i}\frac{\partial A_1(x,y,z;t)}{\partial t} = \Omega_p^* A_3(x,y,z;t), \tag{7a}$$

$$\mathrm{i}\frac{\partial A_2(x,y,z;t)}{\partial t} = f_1 A_2(x,y,z;t) + \Omega_c^* A_3(x,y,z;t), \tag{7b}$$

$$\mathrm{i}\frac{\partial A_3(x,y,z;t)}{\partial t} = \Omega_p A_1(x,y,z;t) + \Omega_c A_2(x,y,z;t) + f_2 A_3(x,y,z;t), \tag{7c}$$

$$\mathrm{i}\frac{\partial A_{e,k}(x,y,z;t)}{\partial t} = f_3 A_{e,k}(x,y,z;t) + g_{k,3e}^* A_3(x,y,z;t), \tag{7d}$$

where $f_1 = \Delta_p - \Delta_c$, $f_2 = \Delta_p - \mathrm{i}\Gamma_0/2$ and $f_3 = \Delta_p - \delta_k$. $\Gamma_0 = 2\pi|g_{k,3e}|^2 D(\omega_k)$ is the spontaneous-decay rate from state $|3\rangle$ to state $|e\rangle$, and $D(\omega_k)$ is the vacuum-mode density at frequency ω_k in the free space. The decay of excited state $|3\rangle$ back to the ground states $|1\rangle$ and $|2\rangle$ are neglected here.

Carrying out the Laplace transformations $\tilde{A}(x,y,z;s) = \int_0^\infty A(x,y,z;t)\mathrm{d}t$ (s is the time Laplace transform variable) for (7a)–(7d), we have the results

$$\mathrm{i}\tilde{A}_1(x,y,z;s)s = \Omega_p^* \tilde{A}_3(x,y,z;s) + \mathrm{i}A_1(0), \tag{8a}$$

$$\mathrm{i}\tilde{A}_2(x,y,z;s)s = f_1\tilde{A}_2(x,y,z;s) + \Omega_c^*\tilde{A}_3(x,y,z;s) + \mathrm{i}A_2(0), \tag{8b}$$

$$\mathrm{i}\tilde{A}_3(x,y,z;s)s = \Omega_p\tilde{A}_1(x,y,z;s) + \Omega_c\tilde{A}_2(x,y,z;s) + f_2\tilde{A}_3(x,y,z;s) + \mathrm{i}A_3(0), \tag{8c}$$

$$\mathrm{i}\tilde{A}_{e,k}(x,y,z;s)s = f_3\tilde{A}_{e,k}(x,y,z;s) + g_{k,3e}^*\tilde{A}_3(x,y,z;s), \tag{8d}$$

where $A_i(0)$ ($i = 1-3$) are initial populations distributed in state $|1\rangle$, $|2\rangle$ and $|3\rangle$, respectively.

Finally, the conditional probability of finding the atom in level $|e\rangle$ with a spontaneously emitted photon of frequency ω_k in the vacuum mode $\boldsymbol{k}$ is then given by

$$W(x,y,z;t\to\infty|e,1_k) = |N|^2|f(x,y,z)|^2|g_k|^2 \times \left|\frac{\Omega_p(f_3-f_1)A_1(0) + \Omega_c f_3 A_2(0) + f_3(f_3-f_1)A_3(0)}{\mathrm{i}f_3(f_2-f_3)(f_3-f_1) + \mathrm{i}|\Omega_p|^2(f_3-f_1) + \mathrm{i}|\Omega_c|^2 f_3}\right|^2. \tag{9}$$

Due to the center-of-mass wave function of the atom $f(x,y,z)$ is assumed to be nearly constant over many wavelengths of the standing-wave fields, the conditional position probability distribution $W(x,y,z;t\to\infty|e,1_k)$ is determined by the filter function defined as

$$F(x,y,z) = \left|\frac{\Omega_p(f_3-f_1)A_1(0) + \Omega_c f_3 A_2(0) + f_3(f_3-f_1)A_3(0)}{\mathrm{i}f_3(f_2-f_3)(f_3-f_1) + \mathrm{i}|\Omega_p|^2(f_3-f_1) + \mathrm{i}|\Omega_c|^2 f_3}\right|. \tag{10}$$

3 Results and discussion

In this section, we investigate the 3D localization behavior of atom by analyzing $F(x,y,z)$ as the filter function which directly reflects the conditional position probability distribution, and then address how the system parameters can be used to achieve 3D atom localization by measuring the spontaneously emitted photon in mode $\boldsymbol{k}$. It is evident from Eq. (10) that $F(x,y,z)$ depends on the initial populations distributed $A_i(0)$ and other parameters of corresponding fields. In the following, we select Γ_0 as the spontaneous decay rate from state $|3\rangle$ to state $|e\rangle$. All the parameters used in numerical calculations are in the unit of Γ_0.

We can see from formula (10) that there is a strong correlation between the detuning of spontaneously emitted photon δ_k and the filter function $F(x,y,z)$. The isosurfaces for the filter function $F(x,y,z) = 0.1$ versus positions ($-1 \le kx/\pi \le 1$, $-1 \le ky/\pi \le 1$, $-1 \le kz/\pi \le 1$) for different values of the detuning of spontaneously emitted photon is plotted in Fig. 2. In the case of the

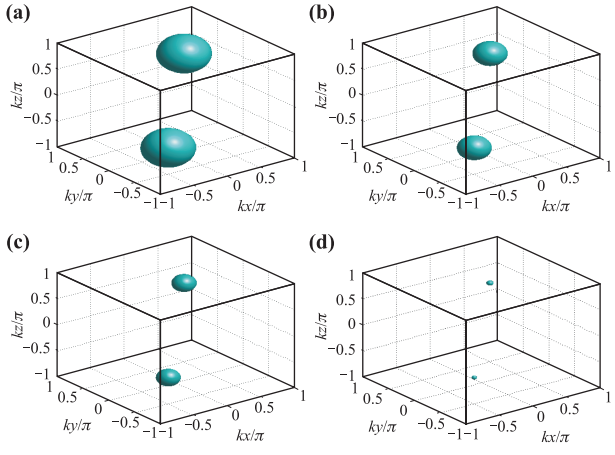

Fig. 2 Isosurfaces for the filter function $F(x,y,z) = 0.1$ versus positions ($-1 \le kx/\pi \le 1$, $-1 \le ky/\pi \le 1$, $-1 \le kz/\pi \le 1$) for different values of δ_k. **(a)** $\delta_k = 26\Gamma_0$; **(b)** $\delta_k = 29\Gamma_0$; **(c)** $\delta_k = 30\Gamma_0$; **(d)** $\delta_k = 31\Gamma_0$. The other parameters are $A_1(0) = A_2(0) = 1/\sqrt{2}$, $A_3(0) = 0$, $\Omega_p = 0.5\Gamma_0$, $\Delta_p = \Delta_c = 0$, $\Omega_1 = \Omega_2 = \Omega_3 = 5\Gamma_0$, $k_1 = k_2 = k_3 = k_4 = k_5 = k_6 = k$, and $\theta_1 = \theta_2 = \theta_3 = 0$.

detuning $\delta_k = 26\Gamma_0$ [see Fig. 2(a)], it can be seen that the isosurfaces of the filter function exhibits two big spheres of the same size in the subspaces ($-1 \le kx/\pi \le 0$, $-1 \le ky/\pi \le 0$, $-1 \le kz/\pi \le 0$) and ($0 \le kx/\pi \le 1$, $0 \le ky/\pi \le 1$, $0 \le kz/\pi \le 1$), respectively. When the detuning δ_k increases to $29\Gamma_0$, the filter function is also situated in two subspaces, but the size of the sphere in each subspace becomes small [see Fig. 2(b)]. Moreover, when the detuning $\delta_k = 30\Gamma_0$, the size of the sphere in each subspace becomes smaller, as shown in Fig. 2(c). Furthermore, when the detuning is detected at an appropriate value (i.e., $\delta_k = 31\Gamma_0$ in Fig. 2(d)), the size of the sphere in each subspace becomes smaller compared to Fig. 2(c). In such a case, we can achieve high-precision and high-resolution 3D atom localization by adjusting the detuning of the spontaneously emitted photon.

In order to further understand the physical mechanisms of the above results in Fig. 2, here we show an alternative explanation for the preceding interesting phenomena of spontaneous emission. By using the dressed-state picture, the bare-state levels $|2\rangle$ and $|3\rangle$ can be replaced by two new states $|-\rangle$ and $|+\rangle$ [see Fig. 1(b)]. The energy eigenstates are written as

$$|+\rangle = \cos(\theta)|3\rangle + \sin(\theta)|2\rangle, \tag{11a}$$

$$|-\rangle = \sin(\theta)|3\rangle - \cos(\theta)|2\rangle, \tag{11b}$$

with $\tan(\theta) = \omega_+/\Omega_c$ and $\omega_\pm = (-\Delta_c \pm \sqrt{\Delta_c^2 + 4\Omega_c^2})/2$ representing frequencies of $|+\rangle$ and $|-\rangle$ relative to level $|0\rangle$.

According to the above dressed states (11a)–(11b), the probability amplitudes of the bare states are associated with the probability amplitudes of the dressed states by the following relations:

$$A_2(x,y,z;t) = \sin(\theta)A_+(x,y,z;t) - \cos(\theta)A_-(x,y,z;t), \tag{12a}$$

$$A_3(x,y,z;t) = \cos(\theta)A_+(x,y,z;t) + \sin(\theta)A_-(x,y,z;t), \tag{12b}$$

Then, Eqs. (7a)–(7d) can be rewritten as

$$\mathrm{i}\frac{\partial A_1(x,y,z;t)}{\partial t} = \Omega_{p+}^* A_+(x,y,z;t) + \Omega_{p-}^* A_-(x,y,z;t), \tag{13a}$$

$$\mathrm{i}\frac{\partial A_-(x,y,z;t)}{\partial t} = \left(\Delta_- - \mathrm{i}\frac{\Gamma_-}{2}\right) A_-(x,y,z;t) + \Omega_{p-} A_1(x,y,z;t) - \mathrm{i}\frac{\Gamma_{+-}}{2} A_+(x,y,z;t), \tag{13b}$$

$$\mathrm{i}\frac{\partial A_+(x,y,z;t)}{\partial t} = \left(\Delta_+ - \mathrm{i}\frac{\Gamma_+}{2}\right) A_+(x,y,z;t) + \Omega_{p+} A_1(x,y,z;t) - \mathrm{i}\frac{\Gamma_{+-}}{2} A_-(x,y,z;t), \tag{13c}$$

$$\mathrm{i}\frac{\partial A_{e,k}(x,y,z;t)}{\partial t} = (\Delta_p - \delta_k) A_{e,k}(x,y,z;t) + g_{k+}^* A_+(x,y,z;t) + g_{k-}^* A_-(x,y,z;t), \tag{13d}$$

with $\Delta_+ = \Delta_p + \omega_+$, $\Delta_- = \Delta_p + \omega_-$, $\Gamma_+ = \Gamma_0 \cos^2\theta$, $\Gamma_- = \Gamma_0 \sin^2\theta$, $\Gamma_{+-} = \Gamma_0 \cos\theta \sin\theta$, $\Omega_{p+} = \Omega_p \cos\theta$, $\Omega_{p-} = \Omega_p \sin\theta$, $g_{k+} = g_{k0} \cos\theta$, $g_{k-} = g_{k0} \sin\theta$.

From Eqs. (13a)–(13d), it is straightforward to show that there exists quantum interference between the two spontaneous-decay channels $|+\rangle \to |e\rangle$ and $|-\rangle \to |e\rangle$ because level $|+\rangle$ interacts with level $|-\rangle$ by spontaneous emission [$(\partial A_+/\partial t) = \cdots - (\Gamma_{+-}/2)A_-$ and $(\partial A_-/\partial t) = \cdots - (\Gamma_{+-}/2)A_+$]. This means that this four-level atom is equivalent to an atom composed of two close-lying upper levels and two well-spaced lower levels [see Fig. 1(b)], and the quantum interference denoted by Γ_{+-} in Eq. (13d) has the same physical meaning as SGC.

In Fig. 3, we study the influence of detuning Δ_c on the 3D atom localization. When the detuning $\Delta_c = 2\Gamma_0$, the filter function is situated in 3D space with two spheres of same size [see to Fig. 3(a)]. Therefore, the probability of finding the atom is 0.5 in one period of standing waves. Interestingly, when the detuning $\Delta_c = -2.15\Gamma_0$ [see Fig. 3(b)], the filter function shows a small-size sphere in the subspace ($0 \le kx/\pi \le 1$, $0 \le ky/\pi \le 1$, $0 \le kz/\pi \le 1$), the spatial resolution is about 0.04λ. That is, the application of a coherent coupling field results in a 1 detecting probability of an atom at a particular position within one period of standing-wave fields. Obviously, the precision of 3D atom localization can be enhanced via the detuning Δ_c.

In Fig. 4, we investigate the influence of the intensity of the coherent controlling field Ω_p on the 3D atom lo-

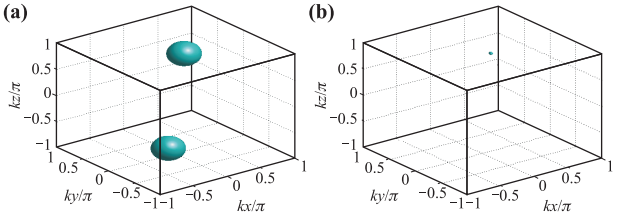

Fig. 3 Isosurfaces for the filter function $F(x,y,z) = 0.1$ versus positions ($-1 \le kx/\pi \le 1$, $-1 \le ky/\pi \le 1$, $-1 \le kz/\pi \le 1$) for different detunings of the coupling field. **(a)** $\Delta_c = 2\Gamma_0$; **(b)** $\Delta_c = -2.15\Gamma_0$. The other parameters are the same as Fig. 2(c).

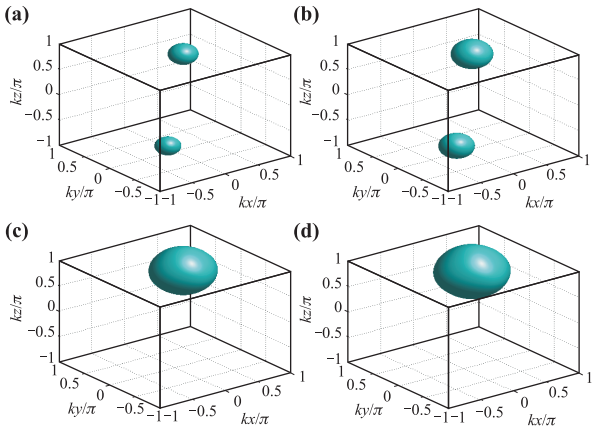

Fig. 4 Isosurfaces for the filter function $F(x, y, z) = 0.1$ versus positions $(-1 \leq kx/\pi \leq 1, -1 \leq ky/\pi \leq 1, -1 \leq kz/\pi \leq 1)$ for different values of the control field. **(a)** $\Omega_p = 5\Gamma_0$; **(b)** $\Omega_p = 10\Gamma_0$; **(c)** $\Omega_p = 18\Gamma_0$; **(d)** $\Omega_p = 20\Gamma_0$. The other parameters are the same as Fig. 2(c).

calization. In the case of $\Omega_p = 5\Gamma_0$, the isosurfaces of the filter function $F(x, y, z)$ are distributed in the subspaces $(-1 \leq kx/\pi \leq 0, -1 \leq ky/\pi \leq 0, -1 \leq kz/\pi \leq 0)$ and $(0 \leq kx/\pi \leq 1, 0 \leq ky/\pi \leq 1, 0 \leq kz/\pi \leq 1)$ with different localization precisions, in which the filter function in the two subspaces shows two small-diameter sphere-like patterns of the same size with a high precision, which leads to the localization of the atom at the two spheres [see Fig. 4(a)]. Moreover, under the condition of $\Omega_p = 10\Gamma_0$, as shown in Fig. 4(b), one can see that the volume of sphere in each subspace becomes bigger. Most interestingly, as we further increase the coupling field Ω_p to $18\Gamma_0$ [see Fig. 4(c)], the sphere $(-1 \leq kx/\pi \leq 0, -1 \leq ky/\pi \leq 0, -1 \leq kz/\pi \leq 0)$ is completely disappeared, and the maxima of the filter function only situated in the subspace $(0 \leq kx/\pi \leq 1, 0 \leq ky/\pi \leq 1, 0 \leq kz/\pi \leq 1)$ with a sphere pattern. In such a condition, the probability of finding the atom in one period of the standing-wave fields is increased to 1, that is to say, the atom can be localized at a particular position and the 3D atom localization is indeed achieved efficiently. Of course, on the condition of $\Omega_p = 20\Gamma_0$, the sphere in the subspace $(0 \leq kx/\pi \leq 1, 0 \leq ky/\pi \leq 1, 0 \leq kz/\pi \leq 1)$ becomes bigger [see Fig. 4(d)], which implies that the increasing controlling field will bring a destructive effect to the precision of 3D atom localization when large detuning of spontaneously emitted photon is considered. Therefore, we obtain the 3D-localization precision is dramatically changed by adjusting the intensity of Ω_p.

To obtain a better understanding of how the initial populations $A_i(0)$ adjust 3D atom localization precision, we plot isosurfaces for the filter function $F(x, y, z) = 0.1$ versus positions $(-1 \leq kx/\pi \leq 1, -1 \leq ky/\pi \leq 1, -1 \leq kz/\pi \leq 1)$ for four different values of the initial population, as shown in Fig. 5. When the atom is initially prepared in state $|3\rangle$, i.e., $A_3(0) = 1$, the isosurfaces of the filter function $F(x, y, z)$ in figure 5(a) exhibit two spheres of the same size in two different subspaces $(-1 \leq kx/\pi \leq 0, -1 \leq ky/\pi \leq 0, -1 \leq kz/\pi \leq 0)$ and $(0 \leq kx/\pi \leq 1, 0 \leq ky/\pi \leq 1, 0 \leq kz/\pi \leq 1)$. When the atom is initially prepared in a superposition state of $|1\rangle$, $|2\rangle$ and $|3\rangle$, i.e., $A_1(0) = A_2(0) = 0.3$, $A_3 = 0.907$, as can be seen from figure 5(b), the isosurfaces for the filter function $F(x, y, z)$ shows a small-size sphere in the subspace $(0 \leq kx/\pi \leq 1, 0 \leq ky/\pi \leq 1, 0 \leq kz/\pi \leq 1)$ and a large-size sphere in the subspace $(-1 \leq kx/\pi \leq 0, -1 \leq ky/\pi \leq 0, -1 \leq kz/\pi \leq 0)$. Interestingly, under the condition of $A_1(0) = 0$, $A_2(0) = A_3(0) = 1/\sqrt{2}$ [see Fig. 5(c)], or $A_1(0) = 0.907$, $A_2(0) = A_3(0) = 0.3$ [see Fig. 5(d)], the isosurfaces for the filter function show a sphere in the subspace $(-1 \leq kx/\pi \leq 0, -1 \leq ky/\pi \leq 0, -1 \leq kz/\pi \leq 0)$. Therefore, the probability of finding the atom at such a position is 1, which is increased by a factor of 4 or 8 compared with the previous schemes [23, 25]. From the above observation, we can understand the role of the initial population $A_i(0)$ on precision in position measurement of the single atom in the 3D space.

A new way for realizing the efficient 3D atom localization is shown in Fig. 6, we investigate the influence of the wave vector k_i $(i = 1, 3, 5)$ on the 3D atom localization. On the condition of $k_1 = k_3 = k_5 = 1.2k$, it can be found from figure 6(a) that two same-size spheres in each subspace $(-1 \leq kx/\pi \leq 0, -1 \leq ky/\pi \leq 0, -1 \leq kz/\pi \leq 0)$ and $(0 \leq kx/\pi \leq 1, 0 \leq ky/\pi \leq 1, 0 \leq kz/\pi \leq 1)$. When the wave vectors k_i $(i = 1, 3, 5)$ increase to $1.3k$ [see Fig. 6(b)], the size of spheres in

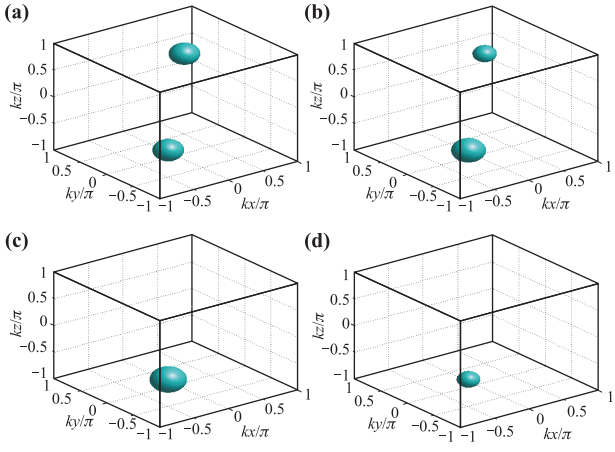

Fig. 5 Isosurfaces for the filter function $F(x, y, z) = 0.1$ versus positions $(-1 \leq kx/\pi \leq 1, -1 \leq ky/\pi \leq 1, -1 \leq kz/\pi \leq 1)$ for different values of initial populations. **(a)** $A_3(0) = 1$, $A_1(0) = A_2(0) = 0$; **(b)** $A_3(0) = 0.907$, $A_1(0) = A_2(0) = 0.3$; **(c)** $A_1(0) = 0$, $A_2(0) = A_3(0) = 1/\sqrt{2}$; **(d)** $A_1(0) = 0.907$, $A_2(0) = A_3(0) = 0.3$. The other parameters are the same as Fig. 2(c).

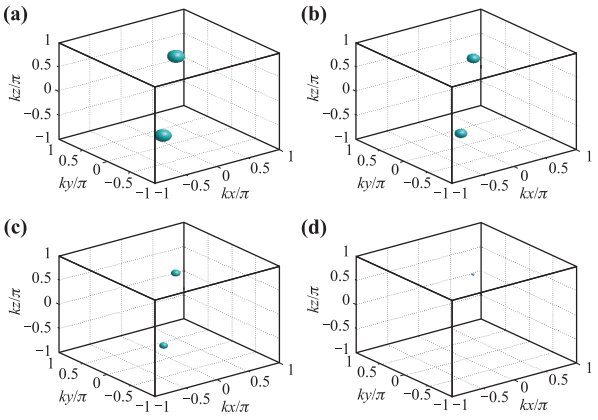

Fig. 6 Isosurfaces for the filter function $F(x, y, z) = 0.1$ versus positions $(-1 \leq kx/\pi \leq 1,\ -1 \leq ky/\pi \leq 1,\ -1 \leq kz/\pi \leq 1)$ for different values of wave vectors. **(a)** $k_1 = k_3 = k_5 = 1.2k$; **(b)** $k_1 = k_3 = k_5 = 1.3k$; **(c)** $k_1 = k_3 = k_5 = 1.36k$; **(d)** $k_1 = k_3 = k_5 = 1.41k$. The other parameters are the same as Fig. 2(c).

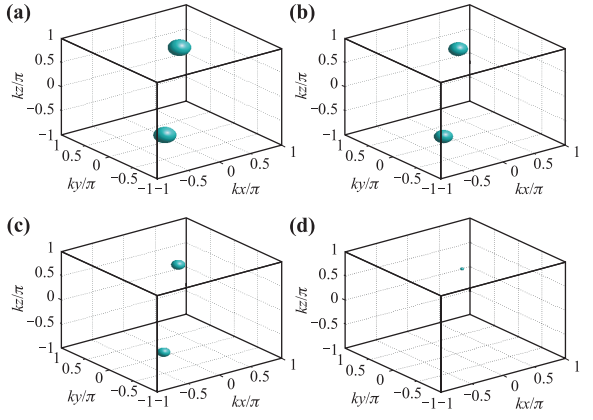

Fig. 7 Isosurfaces for the filter function $F(x, y, z) = 0.1$ versus positions $(-1 \leq kx/\pi \leq 1,\ -1 \leq ky/\pi \leq 1,\ -1 \leq kz/\pi \leq 1)$ for different values of phase shifts. **(a)** $\theta_1 = \theta_2 = \theta_3 = 0$; **(b)** $\theta_1 = \pi/5.9$, $\theta_2 = \theta_3 = 0$; **(c)** $\theta_1 = \theta_2 = \pi/5.9$, $\theta_3 = 0$; **(d)** $\theta_1 = \theta_2 = \theta_3 = \pi/5.9$. The other parameters are the same as Fig. 2(c).

two subspaces is further reduced. As we further increase the wave vectors k_i $(i = 1, 3, 5)$ to $1.36k$, two spheres in the subspaces become very small [see to Fig. 6(c)]. More interestingly, as we further increase the wave vectors k_i $(i = 1, 3, 5)$ to $1.41k$, the sphere $(-1 \leq kx/\pi \leq 0,\ -1 \leq ky/\pi \leq 0,\ -1 \leq kz/\pi \leq 0)$ is completely disappeared and the isosurfaces of the filter function only situated in the subspace $(0 \leq kx/\pi \leq 1,\ 0 \leq ky/\pi \leq 1,\ 0 \leq kz/\pi \leq 1)$ with a sphere pattern [see Fig. 6(d)]. In such a case, the probability of finding the atom at this position is 1, that is, the atom can be localized at a particular position and 3D atom localization is indeed achieved efficiently. In fact, from Eqs. (2) and (10), it is straightforward to show that there is a strong correlation between the wave vectors k_i $(i = 1, 3, 5)$ and the filter function, the varying wave vector influences the spatial distribution of the filter function of $F(x, y, z)$. So we can control the atom localization precision and conditional position probability in 3D space.

Finally, the phase shifts of the relevant fields θ_i $(i = 1 - 3)$ play an important role in the control of the precision of atom localization, as shown in Fig. 7. When $\theta_1 = \theta_2 = \theta_3 = 0$, the isosurfaces for the filter function show two spheres of the same size are situated in two subspaces, respectively [see Fig. 7(a)]. In the case of $\theta_1 = \pi/5.9$, $\theta_2 = \theta_3 = 0$, the localization patterns of the atoms in Fig. 7(b) are still sphere, and the size of the spheres in each subspace becomes smaller. Moreover, when $\theta_1 = \theta_2 = \pi/5.9$ [see Fig. 7(c)], the size of the sphere in each subspace becomes very small. That is to say, the corresponding atom localization precision is further improved compared to Fig. 7(b). Interestingly, when the phase shifts are to changed to $\theta_1 = \theta_2 = \theta_3 = \pi/5.9$, the atom will be localized in subspace $(0 \leq kx/\pi \leq 1,\ 0 \leq ky/\pi \leq 1,\ 0 \leq kz/\pi \leq 1)$ [see Fig. 7(d)]. In such case, the probability of finding the atom in one period of the standing-wave fields is increased to 1. Thus, it is reasonable to achieve the high-precision 3D atom localization in Fig. 7(d).

4 Conclusions

In summary, we investigated 3D atomic localization via spontaneous emission in a coherently-driven, four-level atomic system. Due to spatial-position-dependent atom-field interactions, 3D atom localization can be achieved by measuring spontaneously emitted photons. The precision of 3D atom localization is extremely sensitive to the detuning parameters δ_k and Δ_c, the intensity of the coherent controlling field Ω_p, and the wave vector and phase-shifts of the corresponding standing-wave fields with slightly different wavelengths. More importantly, the maximal probability of finding an atom within a sub-half-wavelength domain of the standing waves can approach 1. As a result, our scheme may be helpful for realizing a spatially selective single-qubit phase gate, entangling gates between cold atoms, and determining the error budget for a single-qubit phase gate in three dimensions.

Acknowledgements This work was supported by the National Natural Science Foundation of China (Grant No. 11674002) and Doctoral Scientific Research Fund of Anhui University.

References

1. G. S. Agarwal, Quantum Optics, edited by G. Höhler, Springer Tracts in Modern Physics Vol. 70, Berlin:

Springer, 1974

2. S. Y. Zhu and M. O. Scully, Spectral line elimination and spontaneous emission cancellation via quantum interference, *Phys. Rev. Lett.* 76(3), 388 (1996)
3. P. Zhou and S. Swain, Quantum interference in probe absorption: Narrow resonances, transparency, and gain without population inversion, *Phys. Rev. Lett.* 78(5), 832 (1997)
4. E. Paspalakis, C. H. Keitel, and P. L. Knight, Fluorescence control through multiple interference mechanisms, *Phys. Rev. A* 58(6), 4868 (1998)
5. E. Paspalakis, N. J. Kylstra, and P. L. Knight, Transparency induced via decay interference, *Phys. Rev. Lett.* 82(10), 2079 (1999)
6. F. Ghafoor, S. Y. Zhu, and M. S. Zubairy, Amplitude and phase control of spontaneous emission, *Phys. Rev. A* 62(1), 013811 (2000)
7. M. A. Antón, O. G. Calderon, and F. Carreno, Spontaneously generated coherence effects in a laser-driven four-level atomic system, *Phys. Rev. A* 72(2), 023809 (2005)
8. E. Paspalakis and P. L. Knight, Phase control of spontaneous emission, *Phys. Rev. Lett.* 81(2), 293 (1998)
9. J. H. Wu, A. J. Li, Y. Ding, Y. C. Zhao, and J. Y. Gao, Control of spontaneous emission from a coherently driven four-level atom, *Phys. Rev. A* 72(2), 023802 (2005)
10. J. H. Li, J. B. Liu, A. X. Chen, and C. C. Qi, Spontaneous emission spectra and simulating multiple spontaneous generation coherence in a five-level atomic medium, *Phys. Rev. A* 74(3), 033816 (2006)
11. A. J. Li, X. L. Song, X. G. Wei, L. Wang, and J. Y. Gao, Effects of spontaneously generated coherence in a microwave-driven four-level atomic system, *Phys. Rev. A* 77(5), 053806 (2008)
12. C. L. Wang, Z. H. Kang, S. C. Tian, Y. Jiang, and J. Y. Gao, Effect of spontaneously generated coherence on absorption in a V-type system: Investigation in dressed states, *Phys. Rev. A* 79(4), 043810 (2009)
13. A. M. Herkommer, W. P. Schleich, and M. S. Zubairy, Autler-Townes microscopy on a single atom, *J. Mod. Opt.* 44(11–12), 2507 (1997)
14. S. Qamar, S. Y. Zhu, and M. S. Zubairy, Atom localization via resonance fluorescence, *Phys. Rev. A* 61(6), 063806 (2000)
15. F. Ghafoor, S. Qamar, and M. S. Zubairy, Atom localization via phase and amplitude control of the driving field, *Phys. Rev. A* 65(4), 043819 (2002)
16. F. Ghafoor, Subwavelength atom localization via quantum coherence in a three-level atomic system, *Phys. Rev. A* 84(6), 063849 (2011)
17. R. G. Wan, J. Kou, L. Jiang, Y. Jiang, and J. Y. Gao, Two-dimensional atom localization via controlled spontaneous emission from a driven tripod system, *J. Opt. Soc. Am. B* 28(1), 10 (2011)
18. R. G. Wan and T. Y. Zhang, Two-dimensional sub-half-wavelength atom localization via controlled spontaneous emission, *Opt. Express* 19(25), 25823 (2011)
19. C. L. Ding, J. H. Li, Z. M. Zhang, and X. X. Yang, Two-dimensional atom localization via spontaneous emission in a coherently driven five-level M-type atomic system, *Phys. Rev. A* 83(6), 063834 (2011)
20. C. L. Ding, J. H. Li, R. Yu, Y. Hao, and Y. Wu, High-precision atom localization via controllable spontaneous emission in a cycle-configuration atomic system, *Opt. Express* 20(7), 7870 (2012)
21. Z. P. Wang and B. Yu, High-precision three-dimensional atom localization via spontaneous emission in a four-level atomic system, *Laser Phys. Lett.* 13(6), 065203 (2016)
22. Z. P. Wang, J. Y. Chen, and B. L. Yu, High-dimensional atom localization via spontaneously generated coherence in a microwave-driven atomic system, *Opt. Express* 25(4), 3358 (2017)
23. J. Chen, F. Song, Z. Wang, and B. Yu, Three-dimensional atom localization via spontaneous emission from two different decay channels, *Laser Phys. Lett.* 15(6), 065205 (2018)
24. V. S. Ivanov, Y. V. Rozhdestvensky, and K. A. Suominen, Three-dimensional atom localization by laser fields in a four-level tripod system, *Phys. Rev. A* 90(6), 063802 (2014)
25. Z. Zhu, W. X. Yang, X. T. Xie, S. Liu, S. Liu, and R. K. Lee, Three-dimensional atom localization from spatial interference in a double two-level atomic system, *Phys. Rev. A* 94(1), 013826 (2016)
26. H. R. Hamedi and G. Juzeliunas, Phase-sensitive atom localization for closed-loop quantum systems, *Phys. Rev. A* 94(1), 013842 (2016)
27. Z. H. Zhu, A. X. Chen, S. P. Liu, and W. X. Yang, High-precision three-dimensional atom localization via three-wave mixing in V-type three-level atoms, *Phys. Lett. A* 380(46), 3956 (2016)
28. D. Zhang, R. Yu, Z. Sun, C. Ding, and M. S. Zubairy, High-precision three-dimensional atom localization via phase-sensitive absorption spectra in a four-level atomic system, *J. Phys. B* 51(2), 025501 (2018)
29. J. H. Li, R. Yu, M. Liu, C. L. Ding, and X. X. Yang, Efficient two-dimensional atom localization via phase-sensitive absorption spectrum in a radio-frequency-driven four-level atomic system, *Phys. Lett. A* 375(45), 3978 (2011)
30. Z. H. Zhu, W. X. Yang, A. X. Chen, S. P. Liu, and R. K. Lee, Two-dimensional atom localization via phase-sensitive absorption-gain spectra in five-level hyper inverted-Y atomic systems, *J. Opt. Soc. Am. B* 32(6), 1070 (2015)